Original Article

Evaluations of the diagnostic performance of ZOOMit diffusion-weighted imaging and conventional diffusion-weighted imaging for breast lesions

Chunjiao Weng[#], Yiwen Yang[#], Ling Yang, Chunhong Hu, Xinxing Ma, Guangzheng Li

Department of Radiology, The First Affiliated Hospital of Soochow University, Suzhou, China

Contributions: (I) Conception and design: X Ma, G Li; (II) Administrative support: L Yang, C Hu; (III) Provision of study materials or patients: X Ma, G Li; (IV) Collection and assembly of data: C Weng, Y Yang; (V) Data analysis and interpretation: C Weng, Y Yang; (VI) Manuscript writing: All authors; (VII) Final approval of manuscript: All authors.

[#]These authors contributed equally to this work.

Correspondence to: Xinxing Ma, MD, PhD; Guangzheng Li, MM, MS. Department of Radiology, The First Affiliated Hospital of Soochow University, No. 188 Shizi Street, Suzhou 215006, China. Email: xinxingma@suda.edu.cn; ligz_@126.com.

Background: Diffusion-weighted imaging (DWI) is valuable in the screening, diagnosis, and grading of breast lesions. However, conventional DWI (C-DWI) is prone to chemical shift and distortion. ZOOMit DWI (Z-DWI), as an advanced magnetic resonance imaging (MRI) technique, applies two spatially selective parallel excitation pulses to focus sampling in the hope of obtaining more valuable information. This study aimed to evaluate and compare the image quality and feasibility of Z-DWI with those of C-DWI in breast lesions.

Methods: The study included 51 patients with breast lesions who underwent breast MRI from May 2021 to February 2022. All patients received Z-DWI and C-DWI sequences, with b values selected as 50 and 800 s/mm^2 (Z-DWI$_{b50}$, Z-DWI$_{b800}$, C-DWI$_{b50}$, and C-DWI$_{b800}$). Apparent diffusion coefficient (ADC) values based on Z-DWI and C-DWI were calculated. For qualitative analysis, four image quality parameters were selected and assessed on a 4-point Likert scale (1 = poor and 4 = excellent). For quantitative analysis, ADC, relative ADC (rADC), signal-to-noise ratio (SNR), contrast-to-noise ratio (CNR), and tumor-to-parenchymal contrast (TPC) values were selected for comparison.

Results: Z-DWI had higher scores compared to C-DWI in terms of lesion conspicuity, anatomical details, distortion and artifacts, and overall image quality (P<0.05). Meanwhile, the agreement between the two readers was reasonably good [intraclass correlation coefficient (ICC) range, 0.360–0.881]. The SNR of Z-DWI$_{b800}$ was better than that of C-DWI$_{b800}$ (P<0.001). The Z-DWI ADC and rADC values of breast lesions were statistically significantly lower than those of C-DWI (mean ADC: P<0.001; rADC; P=0.005).

Conclusions: Z-DWI sequences were shown to have superior image quality. The ADC map of Z-DWI is more conducive to the imaging evaluation of breast lesions.

Keywords: Diffusion-weighted imaging (DWI); ZOOMit; breast lesions

Submitted Mar 29, 2023. Accepted for publication Oct 07, 2023. Published online Nov 07, 2023.
doi: 10.21037/qims-23-415
View this article at: https://dx.doi.org/10.21037/qims-23-415

Introduction

Malignant breast lesions are considered to be the most common disease in women, and breast cancer has a high mortality rate (1). In developed countries, almost 12.4% of women are at risk of developing breast lesions in their lifetime. In developing countries, breast lesions are usually diagnosed at very late stages (2). The high prevalence and the need for early treatment of lesions emphasize the importance of early and accurate imaging and clinical diagnosis.

Breast magnetic resonance imaging (MRI) has been studied and applied due its specific soft-tissue visualization properties. Previous studies have revealed that diffusion-weighted imaging (DWI) has considerable value in the screening, diagnosis, grading, and treatment evaluation of breast lesions (3-5). Functional DWI is based on the degree of freedom of water molecule diffusion, which is sensitive to the microstructure of tissue (6). The quantified apparent diffusion coefficient (ADC) can be used to indicate the nature of breast lesions (7). Conventional DWI (C-DWI) applying single-shot echo planar imaging (SS-EPI) is prone to chemical shifts and distortions due to the limitations of the relatively long sampling times in the phase encoding direction; the inhomogeneity of the magnetic field; and respiratory motion, air, and fat artifacts (8). Applying a 2D spatially selective excitation pulse is effective in reducing these artifacts when a zoomed field of view (FOV) is desired. Active excitation of the desired portion of the imaging in the slice and phase encoding directions shortens the echo chain length, reducing image distortion and other artifacts associated with phase encoding, as described by Saritas *et al.* (9) in spinal DWI. The ZOOMit is a recently developed MRI technique that focuses data sampling by applying two spatially selective parallel excitation pulses, which can be independently adjusted to encode the phase and frequency of each channel, where 2D spatially selective excitation pulse is applied (10,11). ZOOMit not only obtains a precise region of interest (ROI) but also suppresses aliasing artifacts from around the FOV as much as possible. This provides a more homogeneous B1 field, a shorter echo time and scan time, and higher spatial resolution (12,13). With this new DWI technique, more anatomical details can be obtained from the ROIs, the negative effects of folding artifacts minimized, image quality improved, distortion and blurring are reduced, and motion and flow artifacts are avoided (14,15). ZOOMit DWI (Z-DWI) has been used for the prostate, parotid gland, and spine, among other sites (16-18). However, it remains to be determined whether the image quality of Z-DWI is sufficient for breast evaluation.

The purpose of this study was thus to explore and compare the image quality of Z-DWI and C-DWI in breast lesions and to evaluate the feasibility of Z-DWI for clinical application.

Methods

Study population

This retrospective study was conducted in accordance with the Declaration of Helsinki (as revised in 2013) and was approved by the Ethics Committee of the First Affiliated Hospital of Soochow University. The relevant informed consent requirements were obtained from patients.

From May 2021 to February 2022, 58 women with clinically suggestive breast lesions attending our hospital underwent 3.0T MRI either as an outpatient or inpatient. The inclusion criteria were the following: patients with clinically suggestive breast lesions, who underwent MRI [especially C-DWI, Z-DWI, and dynamic contrast-enhanced (DCE) MRI]. In DCE sequences, abnormal masses and abnormal enhancements were present in the unilateral or bilateral breasts according to the Breast Imaging Reporting and Data System (BI-RADS) classification criteria in three aspects: morphology, margins, and signal changes. The exclusion criteria were the following: patients with motion artifacts or *in vitro* artifacts (n=2), patients treated for malignancy (n=5), and patients whose image quality could not be assessed in other cases (n=0). For the patients with multifocal lesions, the lesion showing the largest size on the cross-sectional images was selected for analysis. As a result, 51 eligible women (age range, 18–76 years) were ultimately enrolled in the study for statistical analysis.

MRI scanning

Breast MRI examinations were performed using a Siemens MRI system (MAGNETOM Skyra 3.0T) with a unique 18-channel phased-array breast coil. Patients were placed in the prone position. Multiparameter MRI of the breasts, including T1-weighted, T2-weighted, C-DWI, Z-DWI, and DCE sequences, were performed on the patients. If there were suspicious lesions in both breasts, three imaging sessions on the right and left sides were required in the axial orientation, as Z-DWI can only image a single breast at a

Table 1 Scanning parameters of C-DWI and Z-DWI

Scanning parameter	C-DWI	Z-DWI
Slice orientation	Axial	Axial
TR/TE, ms	10,000/53	4,500/68
Field of view, mm	400×152	180×135
Matrix size	250×95	200×150
Slices	26	20
Slice thickness, mm	5	5
Slice gap, mm	1.5	1.5
Voxel size, mm^3	1.6×1.6×5	0.9×0.9×5
Fat suppression	SPAIR	SPAIR
Acquisition time, min:s	2:57	2:34
B values, s/mm^2	50, 800	50, 800
NSA	1,3	1,3
Diffusion mode	3-scan trace	3-scan trace
Diffusion directions	3	3
iPAT	GRAPPA 2	GRAPPA 2
Orientation	LR × AP	LR × AP

C-DWI, conventional diffusion-weighted imaging; Z-DWI, ZOOMit diffusion-weighted imaging; TR, time to repetition; TE, time to echo; SPAIR, spectral attenuated inversion-recovery; NSA, number of signal averages; iPAT, integrated parallel acquisition technique; GRAPPA, generalized autocalibrating partially parallel acquisition; LR, left/right; AP, anteroposterior.

time. The scanning parameters of C-DWI and Z-DWI are listed in *Table 1*.

The ADC maps for both DWI sequences were automatically generated by Siemens devices through algorithmic calculations. In general, the ADC can be calculated from the acquisition of two different b values, which is a linear regression of the logarithmically transformed signal intensity of the two acquisitions (19). Additionally, since adding acquisitions with different b values significantly lengthens the scan time, two b values are usually used in clinical applications, typically b=50 and 800 s/mm^2.

Image analysis

Qualitative analysis

Two breast radiologists (each with more than 6 years' experience) independently analyzed the MRI images on an image archiving and communication system. An independent double-blind method was used for the two readers throughout the measurement and evaluation processes. The two readers reviewed six sets of images ($C\text{-}DWI_{b50}$, $C\text{-}DWI_{b800}$, $Z\text{-}DWI_{b50}$, $Z\text{-}DWI_{b800}$, conventional ADC, and ZOOMit ADC) in random order and scored them with respect to lesion conspicuity, anatomical details, distortion and artifacts, and overall image quality. For each sequence, a 4-point Likert scale (20) was chosen to qualitatively analyze the image quality (1, poor image clarity and serious distortion or motion artifacts; 2, medium image clarity and relatively heavy distortion or motion artifacts; 3, good image clarity and slight distortion or motion artifacts; 4, excellent image clarity and no distortion or motion artifacts).

Quantitative analysis

A diagnostic radiologist in breast (with 10 years' experience) registered ROIs at the same workstation, and another breast diagnostic radiologist (with 10 years' experience) served as an aid. In case of disagreement, a consensus was reached via discussion prior to ROI selection and outlining, which included calculation of signal-to-noise ratio (SNR), contrast-to-noise ratio (CNR), tumor-to-parenchymal contrast (TPC), and ADC values of the C-DWI and Z-DWI images. C-DWI, Z-DWI, and DCE images were transferred to RadiAnt DICOM Viewer software (https://www.radiantviewer.com). The DCE images were used as a reference for the areas of mass-like enhancement and nonmass-like enhancement, and the ROIs were measured against the high-signal portions of the C-DWI and Z-DWI images, respectively, via manual animation of the circles. The dimension with the largest cross-sectional area of the lesion was selected, with the cystic, necrotic, and hemorrhagic areas being avoided, and ROIs were drawn in the parenchymal component areas. For each measurement, three ROIs were selected to calculate the mean value. These ROIs were replicated in other sequences. For a graphical example of ROI selection, see *Figure 1*.

The SNR, CNR, and TPC values were calculated as follows:

$$SNR = \frac{S_{tumor}}{\sigma_{background}} \quad [1]$$

$$CNR = \frac{\left|S_{tumor} - S_{parenchyma}\right|}{\sqrt{\sigma_{tumor}^{\ 2} + \sigma_{parenchyma}^{\ 2}}} \quad [2]$$

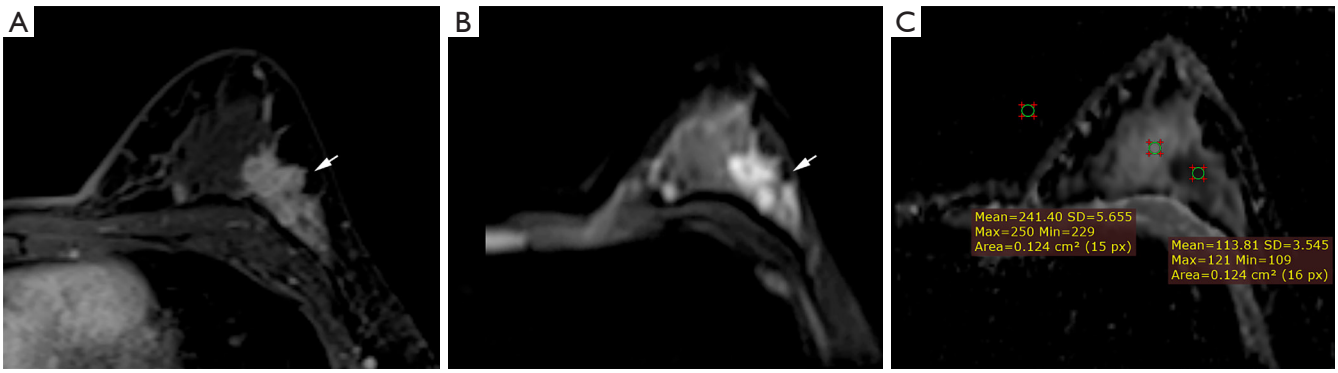

Figure 1 ROI selection for DCE (A), Z-DWI$_{b800}$ and (B) Z-ADC (C). The location of the breast lesion is indicated by the arrow (A,B). DCE images were used as a reference to show either mass-like or nonmass-like enhancement, and then the signals of the lesion (left ROI), normal breast gland (middle ROI), and background noise (right ROI) were measured in each sequence. ROI, region of interest; DCE, dynamic contrast-enhanced; Z-DWI$_{b800}$, ZOOMit diffusion-weighted imaging when b=800 s/mm^2; Z-ADC, ZOOMit ADC; ADC, apparent diffusion coefficient.

$$TPC = \frac{S_{tumor}}{S_{parenchyma}} \quad [3]$$

where S_{tumor} is the signal intensity of the breast lesion, $S_{parenchyma}$ is the signal intensity of the normal breast parenchyma, σ_{tumor} is the standard deviation of the signal intensity of the breast lesion, $\sigma_{parenchyma}$ is the standard deviation of the signal intensity of the normal breast parenchymal, and $\sigma_{background}$ is the standard deviation of the background signal (the air between the breasts).

With RadiAnt DICOM Viewer, axial T1WI-enhanced images and DWI images were used as the reference. Based on the replicated ROIs, the ADC values of each lesion and normal ipsilateral pectoral muscle tissue were similarly measured, and the three ROIs were averaged. In addition, the relative ADC (rADC) value was calculated as an optimization index, which was the mean ADC value of each lesion divided by the mean ADC value of normal ipsilateral pectoral muscle.

Statistical analysis

Statistical analyses were performed using SPSS 26 software (IBM Corp.). After testing for normal distribution, all comparisons used a paired *t*-test or a Wilcoxon signed-rank test. The intraclass correlation coefficient (ICC) with 95% CI was used to assess interreader agreement in terms of qualitative analysis of image quality. An ICC greater than 0.75 indicated excellent interreader agreement (ICC <0.4, poor; ICC 0.4–0.75, fair to good). A P value <0.05 was considered statistically significant.

Results

Qualitative analysis

A total of 51 women were included in the study analysis with a mean age of 43.1 years (SD 11.5 years; range, 18–76 years).

The qualitative parameters of C-DWI and Z-DWI are listed in *Table 2*. Regarding lesion conspicuity, anatomical details, distortion and artifacts, and overall image quality, the two radiologists rated the series of Z-DWI higher compared with the series of C-DWI (*Figures 2,3*). In terms of lesion conspicuity, significant differences were present between C-DWI and Z-DWI (b=50 s/mm^2, ADC) for reader 1 (b=50 s/mm^2: Z=–3.827, P<0.001; ADC: Z=–4.866, P<0.001) and reader 2 (b=50 s/mm^2: Z=–3.199, P=0.001; ADC: Z=–3.826, P<0.001), but no statistical difference existed between C-DWI (b=800 s/mm^2) and Z-DWI (b=800 s/mm^2) (reader 1: Z=–1.667, P=0.096; reader 2: Z=–1.890, P=0.059). Other parameters, including anatomical details, distortion and artifacts, and overall image quality, were significantly different between the six sequences of C-DWI and Z-DWI (both P values <0.05; *Table 2*). Therefore, the Z-DWI sequences generally scored higher in the subjective evaluation of image quality, while b=800 s/mm^2 had the highest score.

The agreement between the two readers with (*Table 3*): b=50 s/mm^2, b=800 s/mm^2, and ADC was reasonably good in terms of lesion conspicuity (C-DWI: 0.881, 0.602, 0.780;

Table 2 Qualitative parameters of C-DWI and Z-DWI

Double reading	Lesion conspicuity	Anatomical details	Distortion and artifacts	Overall image quality
Reader 1				
b=50 s/mm^2				
C-DWI	3.10±0.82	2.00±0.56	2.45±0.54	2.53±0.50
Z-DWI	3.51±0.57	2.63±0.56	2.78±0.46	2.94±0.37
Z	–3.827	–5.166	–3.788	–4.583
P	<0.001	<0.001	<0.001	<0.001
b=800 s/mm^2				
C-DWI	3.55±0.54	2.90±0.45	2.82±0.38	3.02±0.37
Z-DWI	3.65±0.52	3.25±0.52	3.16±0.41	3.47±0.50
Z	–1.667	–4.243	–3.710	–4.796
P	0.096	<0.001	<0.001	<0.001
ADC				
C-ADC	2.90±0.85	1.80±0.69	2.04±0.71	2.35±0.62
Z-ADC	3.53±0.64	2.53±0.57	2.69±0.54	2.92±0.48
Z	–4.866	–5.476	–5.260	–4.874
P	<0.001	<0.001	<0.001	<0.001
Reader 2				
b=50 s/mm^2				
C-DWI	3.22±0.87	1.96±0.39	2.47±0.54	2.67±0.47
Z-DWI	2.65±0.59	2.78±0.46	2.96±0.34	3.92±0.33
Z	–3.199	–5.444	–3.266	–3.873
P	0.001	<0.001	0.001	<0.001
b=800 s/mm^2				
C-DWI	3.82±0.43	2.96±0.34	2.90±0.30	3.12±0.38
Z-DWI	3.92±0.33	3.31±0.50	3.08±0.27	3.51±0.50
Z	–1.890	–4.025	–2.714	–4.264
P	0.059	<0.001	0.007	<0.001
ADC				
C-ADC	3.22±0.89	1.94±0.67	2.10±0.66	2.53±0.57
Z-ADC	3.76±0.51	2.57±0.57	2.71±0.53	2.98±0.31
Z	–3.826	–5.184	–4.670	–4.600
P	<0.001	<0.001	<0.001	<0.001

The values are presented as the mean ± SD. C-DWI, conventional diffusion-weighted imaging; Z-DWI, ZOOMit diffusion-weighted imaging; ADC, apparent diffusion coefficient; C-ADC, conventional ADC; Z-ADC, ZOOMit ADC.

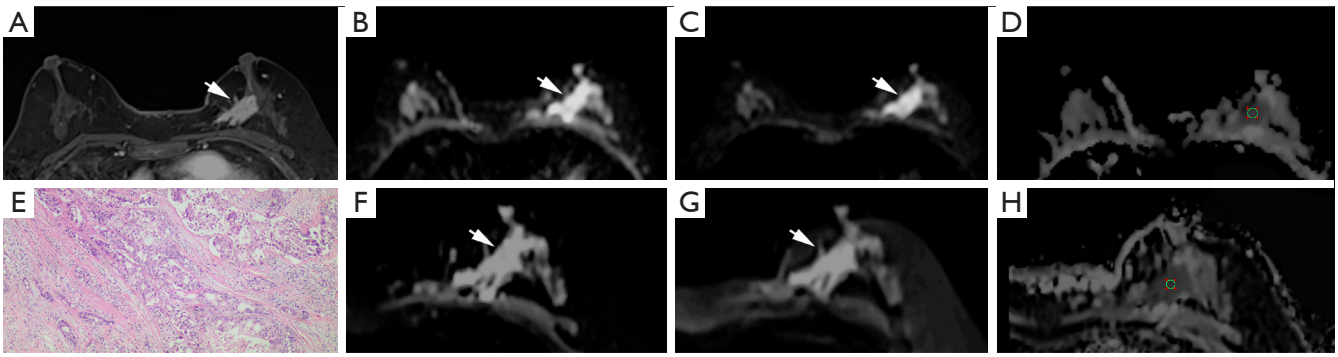

Figure 2 A case of mass-like enhanced lesion (arrows). The patient was a 59-year-old, whose left breast had a mass-like enhanced lesion, which was pathologically confirmed as high-grade ductal carcinoma *in situ*. DCE (A), C-DWI$_{b50}$ (B), C-DWI$_{b800}$ (C), C-ADC (D), hematoxylin eosin staining at 40× (E), Z-DWI$_{b50}$ (F), Z-DWI$_{b800}$ (G), and Z-ADC (H). (B,C,F,G) The signal intensity of the background fibroglandular tissue decreased with increasing b values. Moreover, the lesions on Z-DWI were more distinct and clearer compared to C-DWI both for b=50 and 800 s/mm^2. (F,G) The Z-DWI images show anatomical details of the blur at the edge of the lesion with only minimal artifacts, allowing the lesion to be more easily described. DCE, dynamic contrast-enhanced; C-DWI, conventional diffusion-weighted imaging when b=50 and 800 s/mm^2; C-ADC, conventional ADC; Z-DWI, ZOOMit diffusion-weighted imaging when b=50 and 800 s/mm^2; Z-ADC, ZOOMit ADC; ADC, apparent diffusion coefficient.

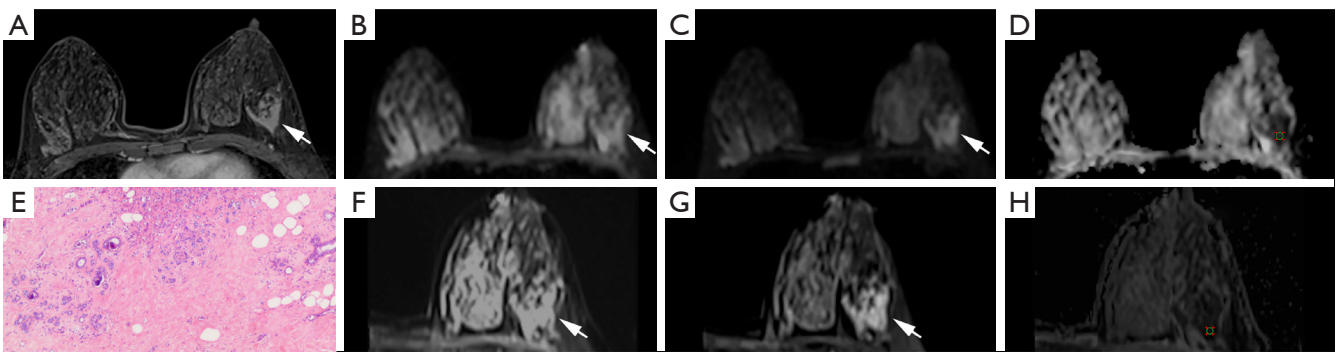

Figure 3 A case of a nonmass-like enhanced lesion (arrows). The patient was a 42-year-old female, whose left breast had a nonmass-like enhanced lesion, which was pathologically confirmed as stage II invasive ductal carcinoma. DCE (A), C-DWI$_{b50}$ (B), C-DWI$_{b800}$ (C), C-ADC (D), hematoxylin eosin staining at 40× (E), Z-DWI$_{b50}$ (F), Z-DWI$_{b800}$ (G), and Z-ADC (H). Compared with C-DWI (B,C), the nonmass-like enhanced lesions on Z-DWI (F,G) showed sharper contours and more detailed flocculent enhancement. (D,H) The same lesion had fewer signal artifacts and lower intensity on the Z-ADC image. DCE, dynamic contrast-enhanced; C-DWI, conventional diffusion-weighted imaging when b=50 and 800 s/mm^2; C-ADC, conventional ADC; Z-DWI, ZOOMit diffusion-weighted imaging when b=50 and 800 s/mm^2; Z-ADC, ZOOMit ADC; ADC, apparent diffusion coefficient.

Z-DWI; 0.799, 0.572, 0.577), anatomical details (C-DWI: 0.671, 0.510, 0.756; Z-DWI: 0.807, 0.746, 0.576), and overall image quality (C-DWI: 0.722, 0.566, 0.670; Z-DWI: 0.760, 0.760, 0.742, respectively) of the C-DWI and Z-DWI images. The ICCs for the summed scores of the different scales were between 0.510 and 0.881. However, there was poor agreement in the distortion and artifacts of C-DWI$_{b50}$ (ICC, 0.360; 95% CI: 0.131–0.637).

Quantitative analysis

The comparison of the quantitative parameters of C-DWI

Table 3 Consistency comparison of the quantitative parameters of C-DWI and Z-DWI between the two readers

Image set	Lesion conspicuity	Anatomical details	Distortion and artifacts	Overall image quality
C-DWI (b=50 s/mm^2)	0.881 (0.791, 0.932)	0.671 (0.423, 0.812)	0.360 (0.131, 0.637)	0.722 (0.513, 0.841)
C-DWI (b=800 s/mm^2)	0.602 (0.249, 0.783)	0.510 (0.142, 0.720)	0.679 (0.444, 0.816)	0.566 (0.251, 0.751)
C-ADC	0.780 (0.581, 0.880)	0.756 (0.575, 0.860)	0.658 (0.400, 0.805)	0.670 (0.426, 0.811)
Z-DWI (b=50 s/mm^2)	0.799 (0.649, 0.855)	0.807 (0.662, 0.890)	0.772 (0.599, 0.870)	0.760 (0.579, 0.863)
Z-DWI (b=800 s/mm^2)	0.572 (0.182, 0.769)	0.746 (0.556, 0.855)	0.548 (0.215, 0.740)	0.760 (0.580, 0.863)
Z-ADC	0.577 (0.266, 0.757)	0.576 (0.253, 0.758)	0.775 (0.605, 0.870)	0.742 (0.549, 0.852)

The values are presented as intraclass correlation coefficient (95% CI). C-DWI, conventional diffusion-weighted imaging; Z-DWI, ZOOMit diffusion-weighted imaging; ADC, apparent diffusion coefficient; C-ADC, conventional ADC; Z-ADC, ZOOMit ADC.

Table 4 Comparison of the SNR, CNR, and TPC parameters between C-DWI and Z-DWI

Image set	SNR	CNR	TPC
b=50 s/mm^2			
C-DWI	869.84±482.16	9.48±9.72	2.14±1.84
Z-DWI	965.47±518.10	10.34±8.52	2.06±1.09
Z	–1.050	–1.228	–1.219
P	0.294	0.219	0.223
b=800 s/mm^2			
C-DWI	345.10±132.28	12.15±8.19	2.59±1.14
Z-DWI	632.01±342.73	13.18±8.13	2.88±1.37
Z	–5.418	–0.874	–1.523
P	<0.001	0.382	0.128

The values are presented as the mean ± SD. SNR, signal-to-noise ratio; CNR, contrast-to-noise ratio; TPC, tumor-to-parenchymal contrast; C-DWI, conventional diffusion-weighted imaging; Z-DWI, ZOOMit diffusion-weighted imaging.

Table 5 Comparison of the ADC values between C-DWI and Z-DWI

Image set	Mean ADC (×10^{-3} mm^2/s)	rADC (×10^{-3} mm^2/s)
C-DWI	1.14±0.40	0.72±0.32
Z-DWI	1.05±0.41	0.67±0.30
Z	–4.340	–2.791
P	<0.001	0.005

The values are presented as the mean ± SD. ADC, apparent diffusion coefficient; C-DWI, conventional diffusion-weighted imaging; Z-DWI, ZOOMit diffusion-weighted imaging; mean ADC, average value of apparent diffusion coefficient (×10^{-3} mm^2/s); rADC, the relative apparent diffusion coefficient (×10^{-3} mm^2/s).

and Z-DWI is summarized in *Tables 4*,*5*.

There were no significant differences between C-DWI$_{b50}$ and Z-DWI$_{b50}$ in terms of SNR (Z=–1.050; P=0.294), CNR (Z=–1.228; P=0.219), or TPC (Z=–1.219; P=0.223). In contrast, for b=800 s/mm^2, there was a significant difference in SNR between C-DWI$_{b800}$ and Z-DWI$_{b800}$ (Z=–5.418; P<0.001), with the latter having a higher SNR. The differences in CNR (Z=–0.874; P=0.382) and TPC (Z=–1.523; P=0.128) were not significant between C-DWI$_{b800}$ and Z-DWI$_{b800}$. Meanwhile, the mean ADC (Z=–4.340; P<0.001) and rADC (Z=–2.791; P=0.005) values were significantly lower for Z-DWI than for C-DWI.

Discussion

DWI is being increasingly used in clinical breast MRI. Tissues with a dense cellular structure are more likely to limit diffusion due to the Brownian motion of water molecules, which can be applied to breast lesions, particularly in breast cancer (21,22). Previous studies have shown that DWI and ADC can increase the specificity of the diagnosis of breast lesions and can be used to characterize tumors (23-25). Recently, the advanced Z-DWI technique was to determine if it can provide additional benefits in diagnostic imaging and clinical utility. Siemens Healthineers created ZOOMit to apply echo-planar imaging and another parallel radiofrequency pulse sequence, thus obtaining a reduced FOV in the phase direction (26). ZOOMit DWI technology images a single breast at a time, with encoding limited to the targeted region, thus reducing acquisition time, increasing spatial resolution and decreasing the number of magnetization rate artifacts (14,27).

This study focused on the imaging value and feasibility of Z-DWI technique in breast lesions. We found that breast DWI based on Z-DWI had significantly higher image quality, higher SNR, and lower mean ADC and rADC values than did that based on C-DWI.

In qualitative analysis, our results showed that both readers scored Z-DWI higher than C-DWI in terms of lesion conspicuity, anatomical details, distortion and artifacts, and overall image quality. As stated above, this can be attributed the ability of Z-DWI to apply two spatially selective excitation pulses in reducing the distortion and physical FOV and in increasing the spatial resolution (14,28). ZOOMit had higher image quality in breast lesions and was better suited to the reading habits of the radiologists, which is consistent with previous research by Sun *et al.* (29). Although no significant difference was found in lesion conspicuity when b=800 s/mm^2, the scores were high in both Z-DWI and C-DWI. Moreover, the scores of each qualitative parameter of Z-DWI$_{b800}$ were higher than those of the other sequences This is in line with studies (30,31) that have shown that high b values can provide better imaging quality and lesion conspicuity in breast MRI, possibly due to the increased suppression of background signal.

In addition, six sequences of Z-DWI and C-DWI showed good interreader agreement (ICC range, 0.510–0.881), indicating that the measurement of these qualitative parameters was sufficiently reliable and repeatable (32). For these sequences, the two readers had different scores for the distortion and artifacts of C-DWI$_{b50}$ (ICC =0.360). A low b value in conventional DWI is less sensitive to tissue diffusion, resulting in poorer intertissue contrast. This difference could also be a result of subjectivity in qualitative evaluation and a preference for image quality and standard definitions. Nevertheless, the agreement of the artifacts of Z-DWI$_{b50}$ was higher than that for those of C-DWI$_{b50}$, further suggesting that the ZOOMit technique in superior for displaying and characterizing lesions.

In quantitative analysis, we found that SNR decreased with an increase in the b value, and the SNR of the lesions on Z-DWI was higher than that on C-DWI (b=800 s/mm^2). This is consistent with reports by Cheng *et al.* (33), who reported that high b values require larger diffusion sensitization gradients and longer echo times, possibly resulting in lower SNRs and longer scanning times. Unexpectedly, however, the SNR of Z-DWI (b=800 s/mm^2) was significantly higher (almost twice as high). Several previous studies have reported differences in SNR of reduced FOV scans in multidisease, multidimensional comparisons. Park *et al.* (34) found that zoomed DWI had more specific detail and higher SNR in breast imaging, and Riffel *et al.* (35) came to the same conclusion in their study on renal imaging. This can be attributed to the combination of the phase coded scaling technique with dynamic and spatially selective radiofrequency pulses. Although some studies have indicated that the SNR of fibroglandular and adipose tissue in reduced-FOV DWI is lower than that in C-DWI (36), the diagnostic performance of reduced-FOV DWI in breast MRI was also excellent and valuable.

It is well known that the quantitative measurement of ADC values can contribute to grading and the differentiating of benign and malignant breast lesions. In general, ADC values correlate with the cellularity and the tumor stroma of breast tumors, and a lower ADC value indicates denser glioma cells (37). The diagnostic stability of only using ADC values for breast lesions is not high. Previous studies have proposed various methods to normalize ADC, such as using normal mammary glands on the same side of the lesion, using normal mammary glands on the opposite side of the lesion, and using the pectoralis major muscle as a reference. The mammary gland is closely related to the female menstrual cycle, endocrine regulation, and hormone levels, among other processes. Compared to the mammary gland, the pectoralis major muscle can relatively minimize the impact and error when used as a reference (38,39). The diagnostic efficacy of rADC-muscle in breast lesions has not been extensively reported upon,

and only Tang *et al.* (39) found some degree of superiority of ADC and rADC-muscle in identifying benign and malignant breast lesions. Our study found that the mean ADC and rADC values were significantly lower for Z-DWI (mean ADC 1.05±0.41; mean rADC 0.67±0.30) than for C-DWI (mean ADC 1.14±0.40; mean rADC 0.72±0.32). This is consistent with the evaluation results of Z-ADC values in endometrial carcinoma reported by Karaca *et al.* (40) and those of distal bile duct strictures reported by Sim *et al.* (41). In our opinion, this difference may be partly explained by the reduction of aliasing artifacts or partial volume effects and the good contrast resolution of Z-DWI. The ZOOMit technique may be able to respond to a more realistic and accurate ADC value for the area of interest or lesion.

Some limitations to our study should be mentioned. First, the sample size selected was comparatively small. Second, differences in ROI placement can directly affect the ADC value results (19), causing diversity in ROI selection, but in this study, relatively reliable mean ADC and rADC values were selected as parameters. Finally, this study was dominated by breast lesions with no histopathological results. It may be worth further comparing the interreader agreement of ADC measurements of Z-DWI and C-DWI. Based on existing results, future studies should be conducted in larger patient populations with a variety subgroup analyses based on size, grade, or other pathological characteristics.

Conclusions

In conclusion, Z-DWI had superior image quality compared to the now commonly used C-DWI in regard to clinical utility. In qualitative analysis, Z-DWI showed higher lesion conspicuity, more anatomical detail, and fewer distortion and artifacts. In quantitative analysis, Z-DWI showed higher SNR and lower mean ADC and rADC values, especially at b=800 s/mm^2.

Thus, the Z-DWI technique is feasible and valuable, and its clinical impact should be evaluated in future studies.

Acknowledgments

Funding: None.

Footnote

Conflicts of Interest: All authors have completed the ICMJE uniform disclosure form (available at https://qims.amegroups.com/article/view/10.21037/qims-23-415/coif). The authors have no conflicts of interest to declare.

Ethical Statement: The authors are accountable for all aspects of the work in ensuring that questions related to the accuracy or integrity of any part of the work are appropriately investigated and resolved. This retrospective study was conducted in accordance with the Declaration of Helsinki (as revised in 2013) and was approved by the Ethics Committee of the First Affiliated Hospital of Soochow University. The relevant informed consent requirements were obtained from the patients.

References

1. Momenimovahed Z, Salehiniya H. Epidemiological characteristics of and risk factors for breast cancer in the world. Breast Cancer (Dove Med Press) 2019;11:151-64.
2. Yadav P, Harit S, Kumar D. Efficacy of high-resolution, 3-D diffusion-weighted imaging in the detection of breast cancer compared to dynamic contrast-enhanced magnetic resonance imaging. Pol J Radiol 2021;86:e277-86.
3. Egnell L, Vidić I, Jerome NP, Bofin AM, Bathen TF, Goa PE. Stromal Collagen Content in Breast Tumors Correlates With In Vivo Diffusion-Weighted Imaging: A Comparison of Multi b-Value DWI With Histologic Specimen From Benign and Malignant Breast Lesions. J Magn Reson Imaging 2020;51:1868-78.
4. Ng'ida FD, Kotoroi GL, Mwangi R, Mabelele MM, Kitau J, Mahande MJ. Knowledge and practices on breast cancer detection and associated challenges among women aged 35 years and above in Tanzania: a case in Morogoro Rural District. Breast Cancer (Dove Med Press) 2019;11:191-7.
5. Jeong S, Kim TH. Diffusion-weighted imaging of breast invasive lobular carcinoma: comparison with invasive carcinoma of no special type using a histogram analysis. Quant Imaging Med Surg 2022;12:95-105.

6. Guo Y, Cai YQ, Cai ZL, Gao YG, An NY, Ma L, Mahankali S, Gao JH. Differentiation of clinically benign and malignant breast lesions using diffusion-weighted imaging. J Magn Reson Imaging 2002;16:172-8.
7. Partridge SC, Nissan N, Rahbar H, Kitsch AE, Sigmund EE. Diffusion-weighted breast MRI: Clinical applications and emerging techniques. J Magn Reson Imaging 2017;45:337-55.
8. Zhang J, Peng H, Wang YL, Xiao HF, Cui YY, Bian XB, Zhang DK, Ma L. Predictive Role of the Apparent Diffusion Coefficient and MRI Morphologic Features on IDH Status in Patients With Diffuse Glioma: A Retrospective Cross-Sectional Study. Front Oncol 2021;11:640738.
9. Saritas EU, Cunningham CH, Lee JH, Han ET, Nishimura DG. DWI of the spinal cord with reduced FOV single-shot EPI. Magn Reson Med 2008;60:468-73.
10. Thierfelder KM, Scherr MK, Notohamiprodjo M, Weiß J, Dietrich O, Mueller-Lisse UG, Pfeuffer J, Nikolaou K, Theisen D. Diffusion-weighted MRI of the prostate: advantages of Zoomed EPI with parallel-transmit-accelerated 2D-selective excitation imaging. Eur Radiol 2014;24:3233-41.
11. Williams SN, McElhinney P, Gunamony S. Ultra-high field MRI: parallel-transmit arrays and RF pulse design. Phys Med Biol 2023. doi: 10.1088/1361-6560/aca4b7.
12. Seeger A, Klose U, Bischof F, Strobel J, Ernemann U, Hauser TK. Zoomed EPI DWI of Acute Spinal Ischemia Using a Parallel Transmission System. Clin Neuroradiol 2016;26:177-82.
13. Wan L, Peng W, Zou S, Shi Q, Wu P, Zhao Q, Ye F, Zhao X, Zhang H. Predicting perineural invasion using histogram analysis of zoomed EPI diffusion-weighted imaging in rectal cancer. Abdom Radiol (NY) 2022;47:3353-63.
14. Labounek R, Valošek J, Horák T, Svátková A, Bednařík P, Vojtíšek L, Horáková M, Nestrašil I, Lenglet C, Cohen-Adad J, Bednařík J, Hluštík P. HARDI-ZOOMit protocol improves specificity to microstructural changes in presymptomatic myelopathy. Sci Rep 2020;10:17529.
15. Fang S, Bai HX, Fan X, Li S, Zhang Z, Jiang T, Wang Y. A Novel Sequence: ZOOMit-Blood Oxygen Level-Dependent for Motor-Cortex Localization. Neurosurgery 2020;86:E124-32.
16. Zhou QQ, Zhang W, Yu YS, Li HY, Wei L, Li XS, He ZZ, Zhang H. Comparative Study between ZOOMit and Conventional Intravoxel Incoherent Motion MRI for Assessing Parotid Gland Abnormalities in Patients with Early- or Mid-Stage Sjögren's Syndrome. Korean J Radiol 2022;23:455-65.
17. Gatidis S, Graf H, Weiß J, Stemmer A, Kiefer B, Nikolaou K, Notohamiprodjo M, Martirosian P. Diffusion-weighted echo planar MR imaging of the neck at 3 T using integrated shimming: comparison of MR sequence techniques for reducing artifacts caused by magnetic-field inhomogeneities. MAGMA 2017;30:57-63.
18. Attenberger UI, Rathmann N, Sertdemir M, Riffel P, Weidner A, Kannengiesser S, Morelli JN, Schoenberg SO, Hausmann D. Small Field-of-view single-shot EPI-DWI of the prostate: Evaluation of spatially-tailored two-dimensional radiofrequency excitation pulses. Z Med Phys 2016;26:168-76.
19. Bickel H, Pinker K, Polanec S, Magometschnigg H, Wengert G, Spick C, Bogner W, Bago-Horvath Z, Helbich TH, Baltzer P. Diffusion-weighted imaging of breast lesions: Region-of-interest placement and different ADC parameters influence apparent diffusion coefficient values. Eur Radiol 2017;27:1883-92.
20. Jebb AT, Ng V, Tay L. A Review of Key Likert Scale Development Advances: 1995-2019. Front Psychol 2021;12:637547.
21. Meyer HJ, Martin M, Denecke T. DWI of the Breast - Possibilities and Limitations. Rofo 2022;194:966-74.
22. Mann RM, Kuhl CK, Moy L. Contrast-enhanced MRI for breast cancer screening. J Magn Reson Imaging 2019;50:377-90.
23. Baltzer P, Mann RM, Iima M, Sigmund EE, Clauser P, Gilbert FJ, Martincich L, Partridge SC, Patterson A, Pinker K, Thibault F, Camps-Herrero J, Le Bihan D; . Diffusion-weighted imaging of the breast-a consensus and mission statement from the EUSOBI International Breast Diffusion-Weighted Imaging working group. Eur Radiol 2020;30:1436-50.
24. Xu M, Tang Q, Li M, Liu Y, Li F. An analysis of Ki-67 expression in stage 1 invasive ductal breast carcinoma using apparent diffusion coefficient histograms. Quant Imaging Med Surg 2021;11:1518-31.
25. Iima M, Honda M, Sigmund EE, Ohno Kishimoto A, Kataoka M, Togashi K. Diffusion MRI of the breast: Current status and future directions. J Magn Reson Imaging 2020;52:70-90.
26. He YL, Hausmann D, Morelli JN, Attenberger UI, Schoenberg SO, Riffel P. Renal zoomed EPI-DWI with spatially-selective radiofrequency excitation pulses in two dimensions. Eur J Radiol 2016;85:1773-7.
27. Tanabe M, Higashi M, Benkert T, Imai H, Miyoshi K,

Kameda F, Ariyoshi S, Ihara K, Ito K. Reduced Field-of-View Diffusion-Weighted Magnetic Resonance Imaging of the Pancreas With Tilted Excitation Plane: A Preliminary Study. J Magn Reson Imaging 2021;54:715-20.
28. Kim H, Lee JM, Yoon JH, Jang JY, Kim SW, Ryu JK, Kannengiesser S, Han JK, Choi BI. Reduced Field-of-View Diffusion-Weighted Magnetic Resonance Imaging of the Pancreas: Comparison with Conventional Single-Shot Echo-Planar Imaging. Korean J Radiol 2015;16:1216-25.
29. Sun K, Zhu H, Xia B, Li X, Chai W, Fu C, Thomas B, Liu W, Grimm R, Elisabeth W, Yan F. Image quality and whole-lesion histogram and texture analysis of diffusion-weighted imaging of breast MRI based on advanced ZOOMit and simultaneous multislice readout-segmented echo-planar imaging. Front Oncol 2022;12:913072.
30. Ahn HS, Kim SH, Kim JY, Park CS, Grimm R, Son Y. Image quality and diagnostic value of diffusion-weighted breast magnetic resonance imaging: Comparison of acquired and computed images. PLoS One 2021;16:e0247379.
31. Bickel H, Polanec SH, Wengert G, Pinker K, Bogner W, Helbich TH, Baltzer PA. Diffusion-Weighted MRI of Breast Cancer: Improved Lesion Visibility and Image Quality Using Synthetic b-Values. J Magn Reson Imaging 2019;50:1754-61.
32. Wang X, Liu D, Jiang S, Zeng X, Li L, Yu T, Zhang J. Subjective and Objective Assessment of Monoenergetic and Polyenergetic Images Acquired by Dual-Energy CT in Breast Cancer. Korean J Radiol 2021;22:502-12.
33. Cheng Q, Ye S, Fu C, Zhou J, He X, Miao H, Xu N, Wang M. Quantitative evaluation of computed and voxelwise computed diffusion-weighted imaging in breast cancer. Br J Radiol 2019;92:20180978.
34. Park JY, Shin HJ, Shin KC, Sung YS, Choi WJ, Chae EY, Cha JH, Kim HH. Comparison of readout segmented echo planar imaging (EPI) and EPI with reduced field-of-VIew diffusion-weighted imaging at 3t in patients with breast cancer. J Magn Reson Imaging 2015;42:1679-88.
35. Riffel P, Michaely HJ, Morelli JN, Pfeuffer J, Attenberger UI, Schoenberg SO, Haneder S. Zoomed EPI-DWI of the pancreas using two-dimensional spatially-selective radiofrequency excitation pulses. PLoS One 2014;9:e89468.
36. Baron P, Wielema M, Dijkstra H, Potze JH, Dorrius MD, Sijens PE. Comparison of conventional and higher-resolution reduced-FOV diffusion-weighted imaging of breast tissue. MAGMA 2023;36:613-9.
37. Parsian S, Giannakopoulos NV, Rahbar H, Rendi MH, Chai X, Partridge SC. Diffusion-weighted imaging reflects variable cellularity and stromal density present in breast fibroadenomas. Clin Imaging 2016;40:1047-54.
38. Nadrljanski MM, Milosevic ZC. Relative apparent diffusion coefficient (rADC) in breast lesions of uncertain malignant potential (B3 lesions) and pathologically proven breast carcinoma (B5 lesions) following breast biopsy. Eur J Radiol 2020;124:108854.
39. Tang W, Chen L, Jin Z, Liang Y, Zuo W, Wei X, Guo Y, Kong Q, Jiang X. The diagnostic dilemma with the plateau pattern of the time-intensity curve: can the relative apparent diffusion coefficient (rADC) optimise the ADC parameter for differentiating breast lesions? Clin Radiol 2021;76:688-95.
40. Karaca L, Özdemir ZM, Kahraman A, Yılmaz E, Akatlı A, Kural H. Endometrial carcinoma detection with 3.0 Tesla imaging: which sequence is more useful. Eur Rev Med Pharmacol Sci 2022;26:8098-104.
41. Sim KC, Park BJ, Han NY, Sung DJ, Kim MJ, Han YE. Efficacy of ZOOMit coronal diffusion-weighted imaging and MR texture analysis for differentiating between benign and malignant distal bile duct strictures. Abdom Radiol (NY) 2020;45:2418-29.

Cite this article as: Weng C, Yang Y, Yang L, Hu C, Ma X, Li G. Evaluations of the diagnostic performance of ZOOMit diffusion-weighted imaging and conventional diffusion-weighted imaging for breast lesions. Quant Imaging Med Surg 2023;13(12):8478-8488. doi: 10.21037/qims-23-415

